Angle-resolved photoemission study of (100), (110), and (111) surfaces of $Cu_{0.9}Al_{0.1}$: Bulk and surface electronic structure of the alloy

H. Asonen, M. Lindroos, and M. Pessa
Department of Physics, Tampere University of Technology, SF-33101, Tampere 10, Finland

R. Prasad, R. S. Rao, and A. Bansil
Department of Physics, Northeastern University, Boston, Massachusetts 02115
(Received 6 January 1982)

We present angle-resolved photoemission spectra from the low-index faces of *Cu*Al single crystals using 16.85- and 21.22-eV radiation, together with the computed bulk electronic structure of the alloy within the framework of the muffin-tin coherent-potential approximation (CPA). The *d*-band complex of Cu is found to suffer shifts of less than 0.1 eV on alloying, whereas the states of *s-p* symmetry are lowered in energy by as much as on the order of 1 eV. The dispersion curve of the uppermost valence band is measured and with the extrapolation of this curve to the Fermi energy (E_F), the Fermi-surface radii along two directions in the (100) mirror plane are deduced in Cu and *Cu*Al. Of the known surface states in Cu, the (100) Tamm state persists in the alloy but the (111) Tamm state appears only as a weak shoulder in the alloy spectra. The Shockley-state bands persist on the (110) as well as the (111) alloy face and are estimated to accommodate approximately 0.03 electrons/atom more in the alloy compared to Cu. The Shockley states are lowered (in relation to E_F) by 0.3—0.4 eV as a result of alloying but the Tamm states are lowered by less than 0.1 eV. The CPA computations are found to be in an overall quantitative accord with the bulk measurements and these calculations also lead to a qualitative understanding of some of the experimental results concerning surface states in the alloy.

I. INTRODUCTION

Angle-resolved photoemission spectroscopy (ARPES) has contributed significantly to the understanding of the surface and bulk electronic structure of perfect crystals.[1,2] The technique is now developed to the point such that it is possible to determine the energy of an individual occupied Bloch level directly and, in fact, such "experimental" valence-band structures within 5—10 eV of the Fermi energy have been obtained for a number of transition and noble metals.[2]

Although the angle-integrated experiment has been used extensively to study disordered alloys, the application of the angle-resolved technique in this connection is quite recent. Only limited ARPES measurements on CuNi (Ref. 3), AgPd (Ref. 4), and CuAl (Refs. 5 and 6) solid solutions have been reported to date in the literature. It should be noted that preparing and cleaning alloy single crystals, necessary for ARPES, normally presents metallurgical difficulties. For example, often during the anneal-sputter cleaning procedure, annealing causes surface enrichment whereas subsequent sputtering results in an amorphous state. Furthermore, it is only during the last few years that the theoretical understanding of a disordered alloy has advanced to the stage where reliable predictions concerning the bulk electronic structure are possible within the framework of the average *t*-matrix (ATA) and the coherent-potential (CPA) approximations.[7] The corresponding treatment of the muffin-tin alloy surface (also involved in the photoemission process) is largely undeveloped at this time, although a good deal of progress towards understanding the surface electronic structure of perfect *d*-band metals has been made.[8]

In this paper we present angle-resolved uv measurements on the low-index faces of *Cu*Al single crystals with a nominal concentration of 10 at.% Al.[9] Our focus is on delineating the characteristic effects on the bulk and surface electronic structure of Cu resulting from the addition of impurities. CPA computations of the complex-energy bands in the alloy are presented and used to interpret the experimental results. The choice of *Cu*Al was

motivated by the facts that the host metal Cu has been studied extensively via ARPES[2,10] and *Cu*Al belongs to the important class of Hume-Rothery alloys. Also, the *Cu*Al crystal permitted particularly easy cleaning by Ar^+-ion bombardment and annealing.

An outline of this paper is as follows. Section II describes the sample preparation and other experimental aspects. Section III gives an account of the relevant theoretical details. Section IV presents and discusses the angle-resolved spectra from (100), (110), and (111) faces of Cu and *Cu*Al. The bulk and the intrinsic surface states are considered, respectively, in Secs. IV A and IV B.

Before summarizing our principal conclusions, we note that the $Cu_{0.9}Al_{0.1}$ crystals showed a degree of surface enrichment. More specifically, the Auger measurements prefer a surface concentration of 13 at. % Al. For this reason and the fact that the photoemission experiment is surface sensitive, we have considered a number of theoretical results for 13 at. % Al, in addition to the bulk computations on the 10 at. % Al alloy. The calculations for 13 at. % Al are more appropriate for comparing the theoretical predictions with observations, especially in those instances where the effects of alloying vary strongly as a function of the impurity concentration. This, in fact, turns out to be the case for the spectral features associated with the states possessing primarily an *s-p* character (e.g., the conduction bands and the Fermi-surface dimensions). In contrast, the differences between the predictions of the 10% and 13% computations with regard to the *d*-like states are relatively smaller and unimportant within the context of this article.

In connection with the bulk states, the $\vec{k}$ values corresponding to the well-defined peaks in Cu and *Cu*Al spectra were determined by using the triangulation (energy coincidence) method discussed in Ref. 11. Therefore, the theoretical and experimental level shifts could be compared directly for a number of initial states. [The discussion of disorder smearing of levels would, in general, require the computation of photoemission intensity profiles (excepting isolated instances),[6] and is considered beyond the scope of this article.] Our conclusion is that the *d*-like states of Cu experience shifts of less than 0.1 eV. In contrast, the levels of *s-p* symmetry are lowered by as much as on the order of 1 eV with respect to the Fermi energy.

Since only two incident uv frequencies were used to induce electron emission, it was not possible to probe the uppermost valence band along the high-symmetry directions, presumably due to the nonavailability of final states; the dispersion curve in the (001) mirror plane could, nonetheless, be measured[10] and, by its extrapolation to the Fermi energy, the Fermi-surface radii in Cu and *Cu*Al were deduced along two different directions in each case. This, to our knowledge, is the first application of ARPES as a Fermi-surface caliper in metals and alloys. These results, despite their preliminary nature, point to the considerable potential of ARPES in this regard.

Turning to the surface electronic structure we find, in accord with earlier measurements, intrinsic states of Tamm-type on the (100) and (111) faces and of Shockley-type on the (110) and (111) faces in Cu. The aforementioned surface states are found to persist in the alloy. We associate a lowering of 0.3 to 0.4 eV in the position of the Shockley states (in relation to E_F), with the effect of alloying; this is substantially greater than the corresponding shift (lowering) of 0.05—0.01 eV for the Tamm states.[6] The dispersion of the Shockley-state bands on the (110) and (111) faces was measured as a function of $\vec{k}_{||}$ and found to be essentially parabolic. On this basis, we estimate that both the (110) and (111) bands accommodate approximately 0.03 electrons/atoms more in the alloy compared to Cu. Many of the preceding observations can be understood, at least qualitatively, in terms of the bulk electronic structure of the host metal and the alloy. Such an analysis is presented and used to gain insight into the characteristic disorder effects as far as possible.

II. EXPERIMENTAL CONSIDERATIONS

The experiments were carried out on a VG scientific ADES 400 spectrometer capable of x-ray photoemission, Auger electron (AES), uv-photoemission, and low-energy electron diffraction (LEED) measurements. The present uv spectra were obtained at an angular resolution of 3° to 4° full opening of the electron beam cone and an energy resolution of approximately 40 meV. A rare-gas discharge lamp producing He I (21.22 eV) and Ne I (16.85 eV) resonance lines was used to induce electron emission.

The *Cu*Al alloy single crystals were grown from 99.999% pure Cu and 99.999% pure Al with the aid of the Bridgman method. The orientation of the crystals along the various symmetry planes was characterized by Laue diffraction. The composition was determined by x-ray microprobe analysis

to be 10 at. % Al with an error of ± 0.2 at. %. No inhomogeneities were found in the x-ray microanalysis within the limit of resolution (~ 1 μm) of the method. We emphasize that the Cu alloys containing less than 9 at. % Al have been shown to possess little, if any, short-range order[12] and that a periodic (superlattice) structure appears in small domains at the much higher concentration of 17 at. % Al.[13] Therefore, it is reasonable to assume that our samples, containing 10 at. % Al, are substantially disordered, although we did not investigate possible short-range ordering effects. In particular, the comparison of our experimental results with the random alloy computations is a meaningful one.

The crystals were polished mechanically and electrochemically and cleaned *in situ* by repeated cycles of heating at 720 K for 15 to 30 min followed by argon-ion bombardment with (600–1000)-eV beam energy for 1 to 20 min at a time. The base pressure of the spectrometer was typically 5×10^{-9} Pa. The crystal structure and the composition of the surface were monitored, respectively, via LEED and AES measurements. The (100) and (110) surfaces of the alloy were easy to clean; upon annealing the Al content in the surface, as determined by the AES measurements, was approximately equal to 13 at. %. The LEED spectra from these surfaces yielded sharp (1×1) patterns indicating that these surfaces were clean and perfect. Thus annealing the samples at the end of the cleaning procedure did not cause any appreciable change in the composition or the crystal structure of the (100) and (110) surfaces. In contrast, the composition and the crystal structure of the (111) surface was affected considerably by annealing and sputtering. Low-energy AES and LEED studies showed that the annealed (111) surface contained approximately 30 at. % Al and exhibited a $(\sqrt{3}\times\sqrt{3})$ $R30°$ Al overlayer structure. This surface could be converted to the normal (1×1) configuration by 600-eV Ar^+-ion bombardment for 2.5 min. This procedure also reduced the Al content in the surface region to approximately the bulk value.

III. THEORETICAL CONSIDERATIONS

Since the theoretical discussion of disorder effects in this article centers primarily around the nature of the complex energy bands in *Cu*Al, an overview of such computations in alloys is appropriate here. For a detailed discussion of the muffin-tin CPA and ATA formalisms we refer the reader to the literature.[14–17]

The single-site approximations, such as the ATA and the CPA, amount to replacing the random alloy by an equivalent ordered crystal of suitably chosen effective atoms. In particular, the quasiparticle spectrum is given by the secular equation[15,18]

$$||t_{\rm eff}^{-1}(E)-B(\vec{k},E)||=0\ , \tag{1}$$

where the determinant is understood to be in the angular-momentum space. Here, $t_{\rm eff}(E)$ denotes the matrix of the on-the-energy-shell elements of the effective atom and $B(\vec{k},E)$ is the matrix of the familiar Korringa-Kohn-Rostoker (KKR) structure functions. In the alloy A_xB_{1-x}, the ATA would correspond to the simple choice

$$t_{\rm eff}=t^{\rm ATA}=\langle t\rangle=xt_A+(1-x)t_B\ ,$$

while the CPA scattering matrix $t^{\rm CPA}$ must be obtained by numerically solving the CPA self-consistency equation. Since the CPA treats the disorder self-consistently, it is generally believed to be a better approximation than the ATA. However, we note that the ATA, despite its simplicity, captures much of the dominant physics of disorder and is known in many cases to be an adequate approximation.[15]

For a perfect A or B crystal, $t_{\rm eff}\rightarrow t_A$ or t_B and Eq. (1) reduces to the usual KKR equation. Equation (1) thus provides a simple conceptual basis for the band theory of random alloys. In practice, it is convenient to fix the value of the wave vector $\vec{k}$ and solve (1) for $E(\vec{k})$. These solutions are real in a perfect crystal but become complex in an alloy, with the imaginary part representing disorder smearing of the quasiparticle states.

The muffin-tin potentials for Cu and Al used in the present calculations were generated on the basis of the Mattheiss's overlapping charge-densities prescription.[19] The atomic configurations of $3d^{10}4s^2$ and $3s^2p^1$ were employed for Cu and Al, respectively. In both cases, the Herman-Skillman charge densities[20] were overlapped on an fcc lattice of lattice constant 6.8309 a.u. The Cu muffin-tin potential is identical to that used in Ref. 21. The effects of lattice expansion were incorporated as in Ref. 18.[22] The alloy muffin-tin zero was semiempirically raised by 0.08 Ry from its average value of -1.1970 Ry in $Cu_{0.9}Al_{0.1}$; this yielded a good agreement between the computed and the measured changes[23] (between Cu and $Cu_{0.9}Al_{0.1}$) in the energy of the transition corresponding to the edge in

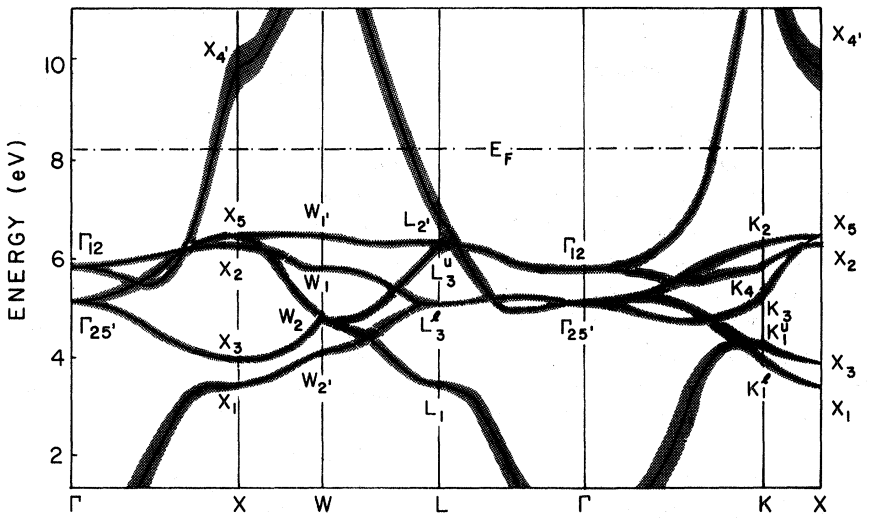

FIG. 1. Complex energy bands in $Cu_{0.9}Al_{0.1}$ along the principal symmetry directions in the Brillouin zone, excluding the effects of lattice expansion (see Ref. 26). The vertical length of shading around the bands equals two times the imaginary part of the complex energies. The energy zero is taken to be -1.1497 Ry, which is the muffin-tin zero for Cu.

the ϵ_2 spectrum (i.e., the vertical transition from the top of the Cu d bands to E_F). We emphasize that such relatively small adjustments in the potentials are generally expected to be necessary in the first-principles band theory of alloys.[18,21] All computations are based on the use of $l \leq 2$ pure-constituent phase shifts. To evaluate the KKR structure functions $B(\vec{k},E)$ efficiently, interpolations in $\vec{k}$ and E were employed.[24,25]

IV. RESULTS

Figure 1 shows the CPA complex-energy solutions of Eq. (1) for $Cu_{0.9}Al_{0.1}$ in the vicinity of the Fermi energy. This underlying alloy spectrum will be used frequently in this section to interpret our experimental results.[26]

A. Bulk electronic structure

The spectra for emission normal to the (100) face are displayed in Fig. 2. The energy bands in Cu along the Γ-X symmetry line (relevant for analyzing these spectra) together with the changes in these bands due to the addition of 10 at. % Al are also shown.

Figure 2(a) shows that, aside from an increased smoothing of the structures in the alloy spectra, the Cu and *Cu*Al spectra are remarkably similar. Note that, in view of Fig. 2(b) and Fig. 1, in the energy range of 2 to 4 eV below E_F (where the spectra are localized), we are primarily probing the Cu d-band complex. The experimental observations therefore imply that the Cu d bands suffer little shift on alloying. This is in accord with the theoretical predictions of Fig. 2(c). Δ_2 and Δ_5 bands, which are d-like, are seen to experience shifts on the order of 0.1 eV; this is also true of the Δ_1 band, except after it develops a significant s-p admixture.

The preceding conclusions were further confirmed by determining the $\vec{k}$ value corresponding to the most pronounced peak in each of the spectra of Fig. 2(a). The triangulation method permitted this determination without any auxiliary assumptions on the band structure.[27] Figure 2(b) shows that the absolute agreement between the measured and calculated levels in Cu is within a few tenths of an eV, as is to be expected for the first-principles computations in the d-band metals. Since our focus is on delineating the disorder effects, we did not attempt to invoke a semiempirical adjustment in the position of the Cu d bands or use a different Cu potential. The *shifts* in the levels due to the addition of impurities are generally insensitive to such uncertainties, and indeed Fig. 2(c) shows that in this regard the theoretical predictions are in good accord with the observations. In particular, the magnitudes of the measured level shifts in Fig. 2(c) are quite small, as anticipated above for the d-like states.

Figures 3 and 4 summarize our results for the

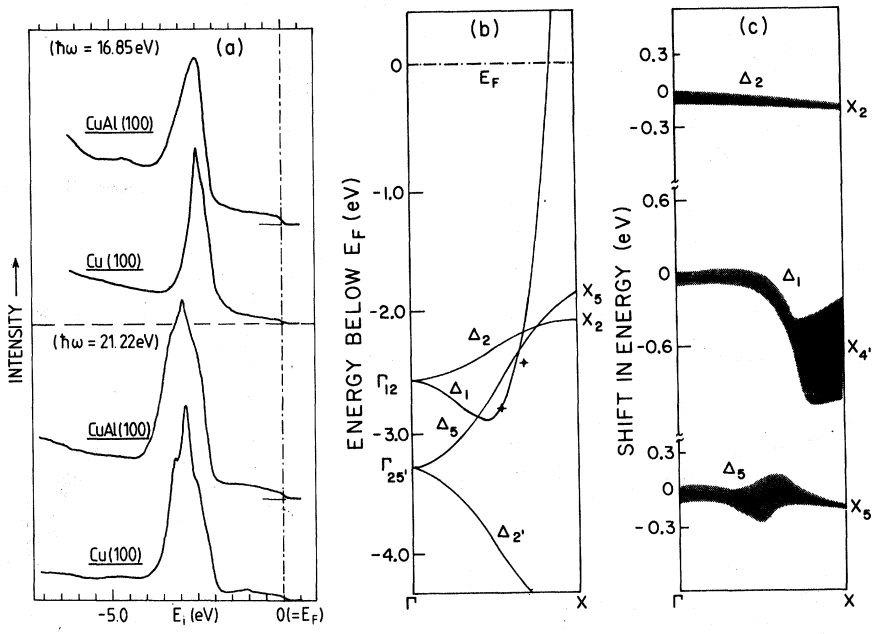

FIG. 2. (a) Photoemission spectra for normal emission from the Cu(100) and *Cu*Al(100) surfaces. (b) Energy bands of Cu along the Γ-*X* direction. The crosses give the E-$\vec{k}$ values corresponding to the most pronounced peak in the two Cu(100) spectra of (a); the horizontal and vertical bars on the crosses represent the $|\vec{k}|$ and E uncertainty. (c) Theoretically computed shift for each of the Cu bands of (b) due to the addition of 10 at. % Al. For the meaning of shading see caption to Fig. 1. Crosses represent experimentally determined level shifts. Note that all curves in (c) give changes *with respect to* E_F.

(110) and the (111) faces, respectively. Much of the discussion presented above in connection with Fig. 2 for the (100) surface is also applicable to these figures with obvious modifications. The normal emission spectra in Figs. 3(a) and 4(a) are seen to be richer in structure than those of Fig. 2(a). Therefore, a larger number of E vs $\vec{k}$ points could be determined experimentally along the *U*-*X* and

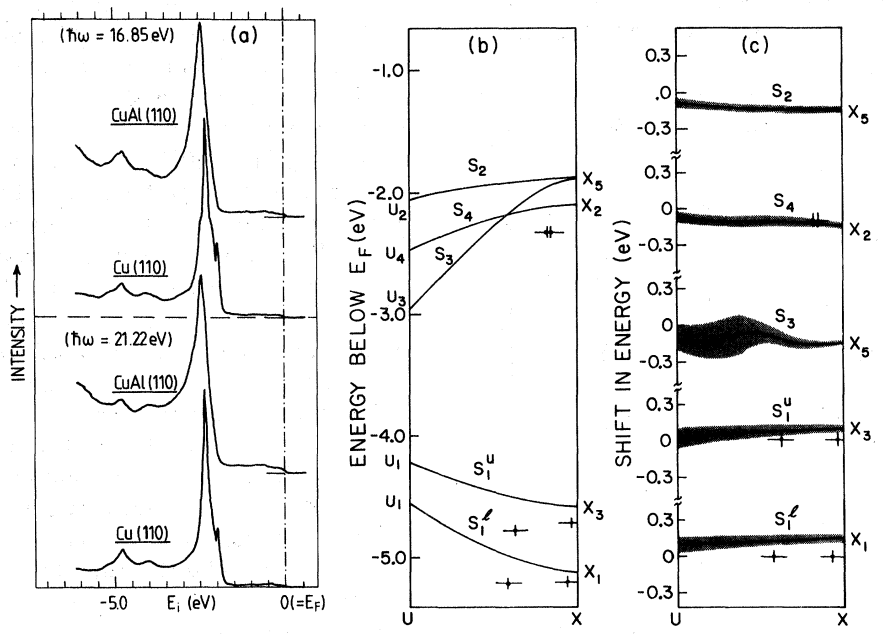

FIG. 3. Same as the caption to Fig. 2, except that this figure displays results for the (110) surface. Experimental spectra are for emission normal to the (110) surface.

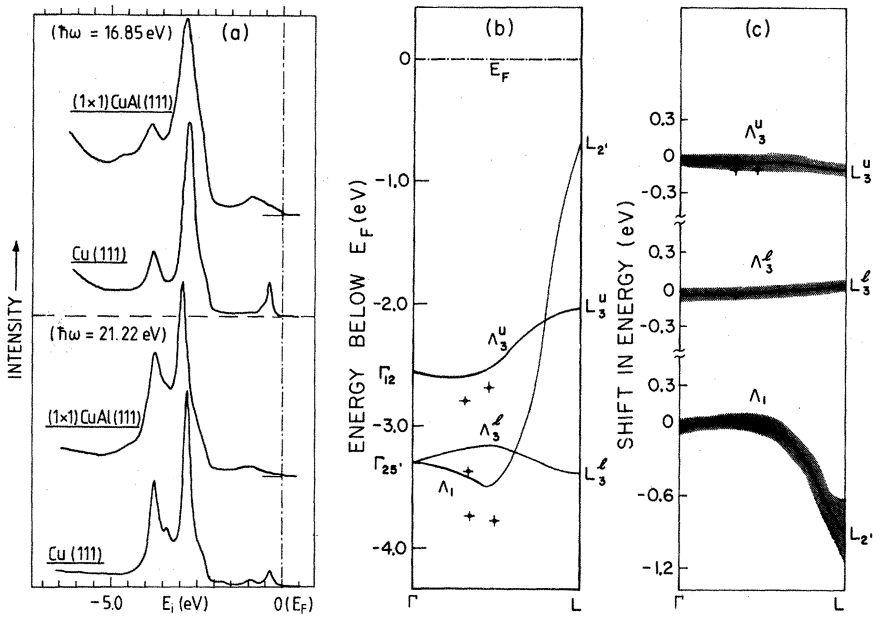

FIG. 4. Same as the caption to Fig. 2, except that this figure displays results for the (111) surface. Experimental spectra are for emission normal to the (111) surface.

the Γ-L directions. [The structure at approximately −0.5 eV in Fig. 4(a) arises from a surface state and is considered in Sec. IV B below.] Figures 2—4 taken together show clearly that the Cu d-states are virtually unaffected by the addition of Al *throughout* the Brillouin zone.

So far we have dealt primarily with the states of d character. As noted in the Introduction, we were unable to probe experimentally the s-p-type states along the principal symmetry directions, apparently because there are no final states available for direct transitions at the two exciting frequencies employed. Figures 1—4 show that much larger level shifts and disorder smearings are predicted theoretically for the levels of s-p symmetry. For example, $X_{4'}$ is lowered (with respect to E_F) by 0.6 eV [Fig. 2(c)] and $L_{2'}$ by 0.9 eV [Fig. 4(c)].

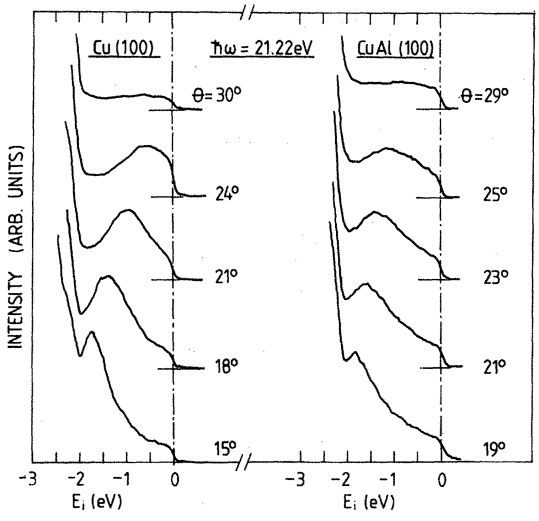

FIG. 5. Angle-resolved spectra from the Cu(100) and *Cu*Al(100) surfaces for 21.22-eV radiation. θ denotes the emission angle with respect to the surface normal.

With this motivation the off-normal emission spectra for the (100) face were also investigated. It has been shown previously[10] that the uppermost filled band of s-p symmetry in Cu can be sampled in this way in the (001) mirror plane [i.e., the (001) plane passing through the center of the Brillouin zone (BZ)]. Figure 5 displays representative 21.22-eV spectra and shows the presence of structures above the d-band edge. The E-$\vec{k}$ values for the peaks in all the 21.22-eV and the 16.85-eV spectra (not shown) were obtained by the triangulation method. The results are shown in Fig. 6, together with the corresponding calculated bands in Cu and *Cu*Al.[28] As noted in the Introduction, the 13% calculation is more relevant in this connection due to the observed surface enrichment in the alloy samples. On the whole, we conclude from Figs. 2(c), 3(c), 4(c), and 6 that the addition of 13% Al lowers the s-p levels in relation to E_F by as much as on the order of 1 eV.

Finally, we present in Fig. 7 all the measured E-$\vec{k}$ points in the (100) mirror plane. The corre-

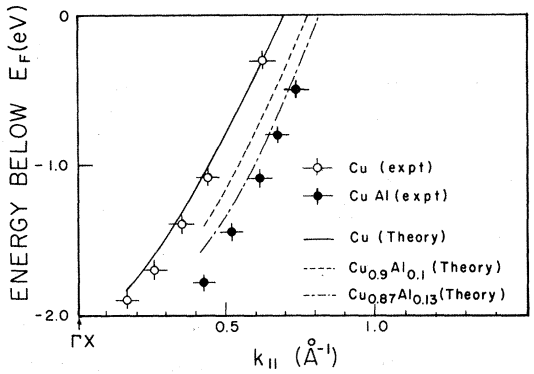

FIG. 6. High-energy conduction bands in Cu and *Cu*Al in the (100) mirror plane. $k_{||}$ denotes the parallel component of $\vec{k}$ along the Γ-X direction. (See Refs. 28, 10, and 11 for details.) The imaginary parts of the alloy complex bands are not shown.

sponding theoretical bands are not shown because various aspects of these measurements have already been considered in detail in the preceding discussion.

By extrapolating the dispersion curves of Figs. 6 and 7 to the Fermi energy, we were able to deduce the Fermi-surface (FS) radii along two directions each in Cu and *Cu*Al. These experimental points, together with the computed cross sections of the Fermi surfaces in the (100) mirror plane are shown in Fig. 8. It is gratifying to see that the Cu points are in accord with the theoretical curve (and the well-known FS of Cu from the de Haas–van Alphen experiments[29]). The 13% Al computations are, once again, seen to be in reasonable agreement with the measurements. Our experiments show

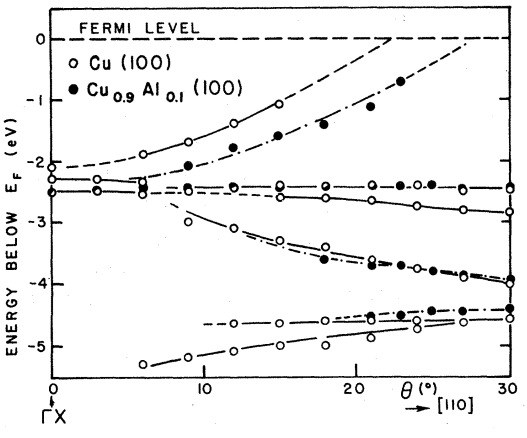

FIG. 7. Experimentally determined "energy bands" in the (100) mirror plane in Cu and *Cu*Al. θ denotes the polar angle of emission with respect to the (100) surface. The dashed lines indicate an extrapolation from the experimental points.

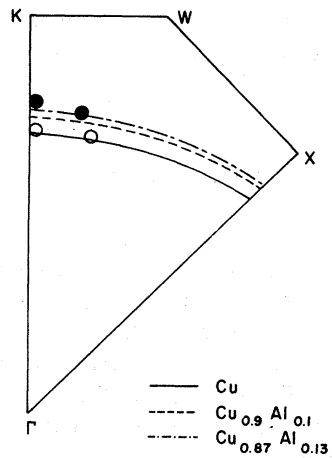

FIG. 8. Theoretically computed intersections of the Fermi surfaces of Cu, $Cu_{0.9}Al_{0.1}$, and $Cu_{0.87}Al_{0.13}$ with the (001) mirror plane in the Brillouin zone. The empty and the filled circles give, respectively, the experimental values for Cu and *Cu*Al as determined by angle-resolved photoemission measurements.

that for measuring the Fermi-surface geometry via ARPES, the surface composition will have to be controlled more carefully than is common in the photoemission work. To develop this application

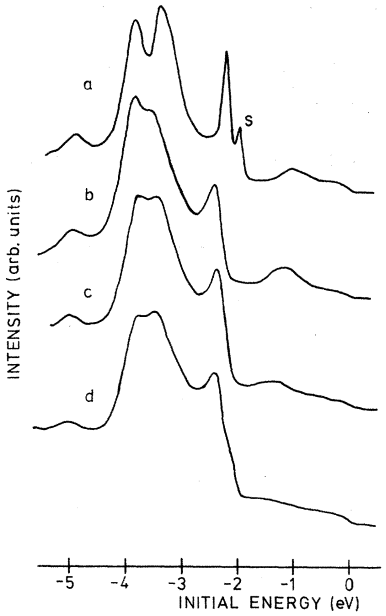

FIG. 9. Photoemission spectra obtained at $\theta = 55°$ and $\hbar\omega = 21.22$ eV for the Cu and *Cu*Al (111) surfaces. *a* spectrum for pure Cu (*S* denotes the structure due to a Tamm-type surface state); *b* *Cu*Al spectrum obtained after annealing the sample at 770 K; *c* *Cu*Al spectrum after the annealed surface was bombarded with Ar^+ ions for 2.5 min at the beam energy of 600 eV; *d* *Cu*Al spectrum after the annealed surface was bombarded with Ar^+ ions for 1.5 min.

of ARPES fully, the use of synchrotron source for inducing electron emission will also be necessary.

B. Surface electronic structure

Tamm-type states which are known to exist on the (100) and (111) faces of Cu are considered first.[30] The (100) surface state persists in *Cu*Al at the $\bar{M}$ symmetry point of the surface Brillouin zone (SBZ). A detailed discussion of the level shift and the disorder smearing of the (100) Tamm state in *Cu*Al has already been presented in Ref. 6; this surface state will therefore not be considered further here. The (111) Tamm state, which was reported to be absent in Ref. 5, is considered in greater detail. Figure 9 shows the relevant spectra from Cu and several alloy single crystals with different surface treatments. Although the (111) Tamm state is seen clearly in Cu (curve *a*), it is only discernible as a weak shoulder around -2.1 eV in one of the alloy samples. (See curve *d* in Fig. 9; the details of this curve are shown in Fig. 10.) The close proximity of the bulk features, together with the broadening of the peaks due to various mechanisms (e.g., disorder, natural linewidth, surface defects, etc.) is probably responsible for the fact that the (111) Tamm state is not well resolved in the alloy spectra.

Figure 10 indicates that the (111) Tamm state is shifted to a higher binding energy by somewhat less than 0.1 eV. We have shown previously that the corresponding shift for the (100) Tamm state amounts to 0.08 eV. We conclude then that a shift of $\lesssim 0.1$ eV represents a characteristic effect of alloying on the Tamm states in Cu.

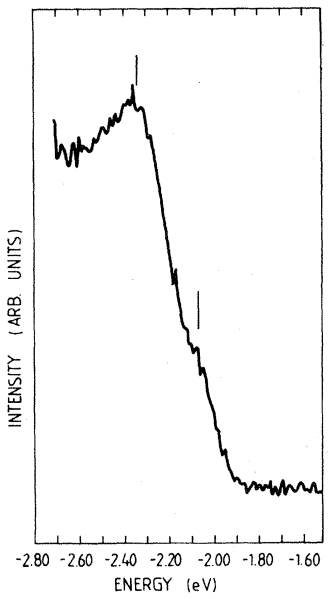

FIG. 10. The details of the curve *d* in Fig. 9.

The Shockley-type states are considered now. Such states, which are known to exist on the (110) and (111) faces of Cu (Ref. 31) were found to persist on the corresponding alloy surfaces in *Cu*Al. On the (111) surface, the Shockley state is localized at $\bar{\Gamma}$ point in the SBZ, and is seen in the normal emission spectra of Fig. 4. The spectra of Fig. 11 further clarify the nature of this state.[32] In particular the bottom of the surface-state band is seen to be lower by 0.4 eV for (1×1) *Cu*Al and by 0.8 eV for $\sqrt{3}\times\sqrt{3}$ *Cu*Al in comparison to Cu(111). The sensitivity of this state to surface conditions is thus obvious. To isolate disorder effects, it is useful to consider the Shockley states associated with the (110) surfaces of Cu and *Cu*Al (see Fig. 12). As emphasized in Sec. II, the (110) surface in contrast to the (111) alloy surface does not exhibit any appreciable changes in the structure or the composition on annealing. The dispersion curves of Fig. 12 show that the bottom of the related surface state band (centered at $\bar{Y}$ in the SBZ, is lowered by 0.33 eV by alloying. This is in good accord with the aforementioned shift of 0.4 eV for the (1×1) CuAl(111) surface. It is reasonable therefore to conclude that the Shockley-type states are lowered by 0.3 to 0.4 eV on adding 13 at. % Al and that this shift represents a characteristic alloying effect.

Since the Shockley states are positioned within the gaps in the bulk band structures the observed movements in their positions can be understood qualitatively in terms of the host and the alloy bulk electronic structures. The gaps of interest in the present case arise from the mixing of states possessing primarily an *s-p* character [e.g., the $L_{2'}$ to L_1^u gap which is relevant for the (111) Shockley state]. Therefore, the associated surface states would also possess a significant *s-p* character and the changes in the energy of the bulk states of this symmetry would be reflected in the corresponding changes in the surface states. We calculate the $L_{2'}$ and L_1^u levels to be lowered by 0.9 and 1.4 eV, respectively, in $Cu_{0.9}Al_{0.1}$ in relation to Cu (Ref. 33); the average shift of 1.15 eV thus obtained is to be compared with the observed value of $0.3-0.4$ eV.[34] The discrepancy may be related to the fact that a surface atom possesses a smaller number of nearest neighbors compared to a bulk atom, and the surface states may therefore be expected to ex-

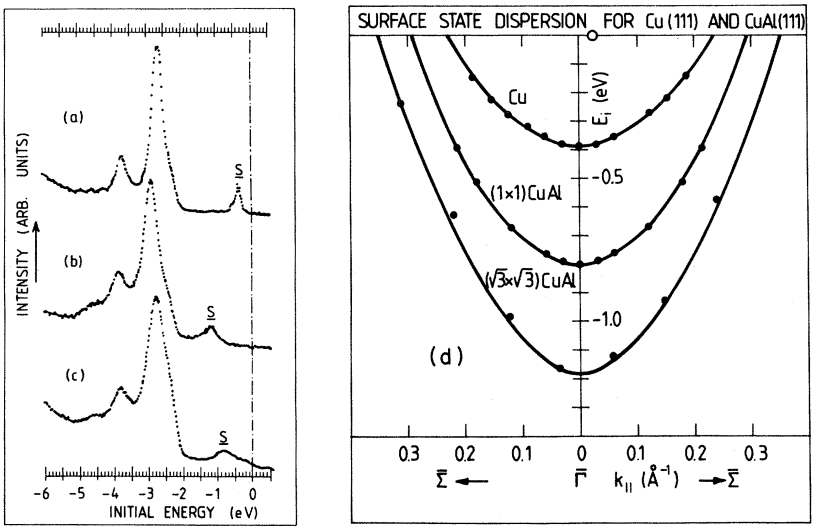

FIG. 11. Normal emission spectra using 16.85-eV radiation from (111) faces of (a) Cu; (b) $\sqrt{3}\times\sqrt{3}$ *Cu*Al with approximately 30 at. % surface concentration of Al, and (c) (1×1) *Cu*Al with approximately 10 at. % surface content of Al. (*S* denotes the structure due to a Shockley-type surface state.) (d) The dispersion curves for the Shockley-state bands for Cu(111), (1×1) *Cu*Al(111), and $(\sqrt{3}\times\sqrt{3})$ *Cu*Al(111).

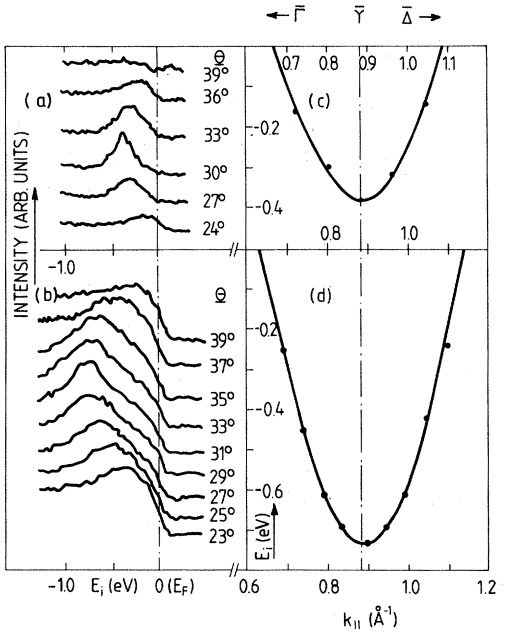

FIG. 12. Angle-resolved spectra from the (110) surface in (a) Cu, and (b) *Cu*Al, for various polar angles (θ) of emission using the 16.85-eV radiation. The dispersion curves for the Shockley-state peaks in (a) and (b) are plotted in (c) and (d) for Cu(110) and *Cu*Al(110), respectively.

perience smaller level shifts compared to the relevant bulk states.

By assuming an isotropic parabolic shape, we have estimated the total number of electrons in the Shockley-state bands of Figs. 11 and 12. On this basis, we obtain the following occupation numbers (in units of electrons/atom): Cu(111)=0.045, (1×1) *Cu*Al(111)=0.075, $(\sqrt{3}\times\sqrt{3})$ *Cu*Al(111) =0.110, Cu(110)=0.070, and *Cu*Al(110)=0.100. By comparing Cu and CuAl both the (110) and (111) bands are seen to accommodate 0.03 electrons/atom more in the alloy [using the (1×1) *Cu*Al(111) data]. These results show that, as in the case of level shifts considered in the preceding paragraph, the *changes* associated with alloying for the Shockley states on the (110) and (111) faces are similar.

As indicated in the Introduction, the question of disorder smearing is generally considered beyond the scope of this article. Nonetheless, it is noteworthy in connection with Fig. 11 that broadening of the spectral features can be sensitive to the surface treatment. A comparison of the curves labeled (b) and (c) in this figure reveals, for example, that the bombarded surface shows features that are broader even though this surface contains less Al. This phenomenon is not related

to disorder-induced smearing but is more likely a result of the crystal defects introduced by bombardment. A similar effect of the crystal imperfections was found earlier in photoemission from AgPd single crystals.[4]

Finally, we note that we have found an unexpected spectral feature at -4.65 eV in emission from the alloy samples. This feature is not present in Cu and is clearly visible in the (100) and (111) *Cu*Al spectra in Figs. 2 and 4. The fact that this feature exhibits no clear dispersion as the emission angle or the incident frequency is varied makes it unlikely that it is associated with the bulk Bloch-type states. Furthermore, this feature is seen in the spectra of the overlayer as well as the normal surface and survives after oxygen absorption and gentle Ar^+-ion bombardment. For these reasons it is also unlikely to be associated with a surface state, even though it does lie energetically within the *s-d* hybridizational gap in the Γ-*L* and Γ-*X* directions in the alloy. As emphasized in Ref. 15, the energy spectrum of the alloy will in general contain *non*-Bloch-type contributions from the complex impurity levels associated with a single Cu or Al atom placed in the effective medium. This possibility was investigated but no such theoretical single impurity levels were found in the relevant energy range. Perhaps the observed spectral feature around -4.65 eV is related to the properties of clusters of more than one atom in the alloy.

ACKNOWLEDGMENTS

We thank Mrs. Paula Huttunen for her assistance in the experiments. Financial support from the Academy of Finland and the U. S. Department of Energy is acknowledged.

[1]N. V. Smith, in *Photoemission in Solids I,* edited by M. Cardona and L. Ley (Springer, Berlin, 1978), p. 237.

[2]D. E. Eastman and F. J. Himpsel, in *Physics of Transition Metals, 1980,* edited by P. Rhodes (Institute of Physics, Bristol, 1981), p. 115.

[3]P. Heimann, H. Neddermeyer, and M. Pessa, Phys. Rev. B 17, 427 (1978); P. Heimann, J. Hermanson, H. Miosga, and H. Neddermeyer, Solid State Commun. 37, 519 (1981).

[4]M. Pessa, H. Asonen, M. Lindroos, A. Pindor, B. L. Gyorffy, and W. Temmerman, J. Phys. F 11, L33 (1981).

[5]H. Asonen and M. Pessa, Phys. Rev. Lett. 46, 1696 (1981).

[6]M. Pessa, H. Asonen, R. S. Rao, R. Prasad, and A. Bansil, Phys. Rev. Lett. 47, 1223 (1981).

[7]A. Bansil, Phys. Rev. Lett, 41, 1670 (1978); G. M. Stocks, W. M. Temmerman, and B. L. Gyorffy, Phys. Rev. Lett. 41, 339 (1978).

[8]W. Kohn, Phys. Rev. B 11, 3756 (1975); N. Kar and P. Soven, *ibid.* 11, 3761 (1975).

[9]The question of the existence of surface states on $Cu_{0.9}Al_{0.1}$(111) was discussed in Ref. 5, which reported that the Cu(111) Shockley state persists in the alloy whereas the Cu(111) Tamm state does not. The observation of the Tamm-type surface state on the $Cu_{0.9}Al_{0.1}$(100) face was reported in Ref. 6.

[10]M. Lindroos, H. Asonen, M. Pessa, and N. V. Smith, Solid State Commun. 39, 285 (1981).

[11]M. Pessa, Solid State Commun. 39, 605 (1981); E. O. Kane, Phys. Rev. Lett. 12, 97 (1964); P. O. Nilsson and N. Dahlback, Solid State Commun. 29, 303 (1979).

[12]M. S. Wechsler and R. H. Kernohan, J. Phys. Chem. Solids 7, 307 (1958); Acta Metall. 7, 599 (1959).

[13]J. B. Andrews, R. J. Nastasi-Andrews, and R. E. Hummel, Phys. Rev. B 22, 1837 (1980).

[14]For recent discussions and further literature citations on the subject of muffin-tin alloys, see Refs. 15 through 17. An early review is to be found in Sec. IX of H. Ehrenreich and L. Schwartz, in *Solid State Physics,* edited by H. Ehrenreich, F. Seitz, and D. Turnbull (Academic, New York, 1976), Vol. 31.

[15]A. Bansil, Phys. Rev. B 20, 4025 (1979); 20, 4035 (1979).

[16]P. E. Mijnarends and A. Bansil, Phys. Rev. B 19, 2919 (1979); A. Bansil, R. S. Rao, P. E. Mijnarends, and L. Schwartz, *ibid.* 23, 3608 (1981).

[17]J. S. Faulkner and G. M. Stocks, Phys. Rev. B 21, 3222 (1980); B. E. A. Gordon, W. E. Temmerman, and B. L. Gyorffy, J. Phys. F 11, 821 (1981).

[18]A. Bansil, H. Ehrenreich, L. Schwartz, and R. E. Watson, Phys. Rev. B 9, 445 (1974).

[19]L. F. Mattheiss, Phys. Rev. 133, A1399 (1964).

[20]F. Herman and S. Skillman, *Atomic Structure Calculations* (Prentice-Hall, Englewood Cliffs, New Jersey, 1963).

[21]R. Prasad, S. C. Papadopoulos, and A. Bansil, Phys. Rev. B 23, 2607 (1981).

[22]See, in particular, footnote 40 of Ref. 21. With the addition of 10 at. % Al, the lattice constant of Cu increases by 0.67%.

[23]R. J. Nastasi-Andrews and R. E. Hummel, Phys. Rev. B 16, 4314 (1977).

[24]The Brillouin-zone integrations, necessary for solving the muffin-tin CPA equation, were carried out by us-

ing the special directions method; the set of 21 special directions was employed (see Ref. 25 for details). The parameters for interpolation of the KKR structure functions (in $\vec{k}$ and E) are identical to those used in Ref. 15.

[25]R. Prasad and A. Bansil, Phys. Rev. B 21, 496 (1980).

[26]The effect of lattice expansion is not included in the complex-energy bands of Fig. 1. In actual comparisons with the experiments, however, the appropriately corrected values are used throughout this article; in particular, this is true of the theoretical curves in Figs. 2—4, 6, and 8.

[27]Within the experimental error, the $\vec{k}$ value for each of the exciting frequencies was found to be the same for Cu and *Cu*Al.

[28]Note that these $\vec{k}$ points do not lie on a straight line in the Brillouin zone. For details, see Refs. 10 and 11.

[29]M. R. Halse, Philos. Trans. R. Soc. London, Ser. A 265, 507 (1962).

[30]P. Heimann, J. Hermanson, H. Miosga, and H. Neddermeyer, Phys. Rev. Lett. 42, 1782 (1979); Phys. Rev. B 20, 3059 (1979).

[31]P. O. Gartland and B. J. Slagsvold, Phys. Rev. B 12, 4047 (1975); P. Heimann, J. Hermanson, H. Miosga, and H. Neddermeyer, Surf. Sci. 85, 263 (1979).

[32]Much of Fig. 11 is reproduced from Ref. 5 for the convenience of discussion. The (1×1) CuAl curve in Fig. 11(d), however, presents new measurements.

[33]The bottom of the Shockley-state band therefore continues to stay well above the $L_{2'}$ level in the alloy.

[34]The shift of 0.3—0.4 eV in the Shockley-state bands is much larger than the corresponding shift of 0.05—0.1 eV for the Tamm states. This is consistent with our observation that the Shockley state possesses an *s-p*-like character whereas the Tamm states arise from the bulk *d* states. As discussed in the text, the states of *d* symmetry experience shifts of less than 0.1 eV on alloying.